Biointerface Research in Applied Chemistry
Open-Access Journal (ISSN: 2069-5837)

Article
Volume 13, Issue 1, 2023, 63
https://doi.org/10.33263/BRIAC131.063

Biosynthesis of Gold Nanoparticles Using *Strobilanthes crispa* Aqueous Leaves Extract and Evaluation of Its Antibacterial Activity

Nur Fatini Samsulkahar [1], Atieya Abdul Hadi [2], Mustaffa Shamsuddin [1,*], Nik Ahmad Nizam Nik Malek [3]

[1] Department of Chemistry, Faculty of Science, Universiti Teknologi Malaysia (UTM), 81310 Skudai, Malaysia; nurfatinisamsul@gmail.com (N.F.S.);
[2] Department of Biosciences, Faculty of Science, Universiti Teknologi Malaysia (UTM), 81310 UTM Johor, Malaysia; atieya@graduate.utm.my (A.A.H.);
[3] Centre for Sustainable Nanomaterials (CSNano), Ibnu Sina Institute for Scientific and Industrial Research (ISI-ISIR), Universiti Teknologi Malaysia (UTM), 81310 UTM Johor, Malaysia; niknizam@utm.my (N.A.N.N.M.);
* Correspondence: mustaffa@kimia.fs.utm.my (M.S.);

Scopus Author ID 8385195200
Received: 22.11.2021; Accepted: 20.12.2021; Published: 2.02.2022

Abstract: The role of plant phytochemicals has drawn undeniable attention for synthesizing stable and eco-friendly nanoparticles. Therefore, this work explores using locally grown *Strobilanthes crispa* aqueous leaves extract for the biosynthesis of gold nanoparticles (AuNPs) using $HAuCl_4$ as the metal precursor. The AuNPs were characterized using Ultraviolet-visible (UV-Vis) spectroscopy, Fourier transforms infrared (FTIR) spectroscopy, High-resolution Transmission electron microscopy (HRTEM), and X-ray diffraction (XRD). The UV-Vis spectrum exhibits two absorption peaks due to surface plasmon resonance of gold at 530 nm and 708 nm within 2 hours. The HRTEM micrographs proved that AuNPs were predominantly spherical with mixtures of anisotropic nanoshapes. The FTIR spectra evident the presence of phytochemical compounds, which acted as the capping agent. The face-centered cubic (fcc) structure was confirmed using the XRD pattern with an average crystallite size of 9.3 nm. The antibacterial assay exhibited a positive inhibitory effect on Gram-negative bacteria (*Escherichia coli* ATCC 11229) compared to Gram-positive bacteria (*Staphylococcus aureus* ATCC 6538). Further *in silico* analysis between AuNPs and *E. coli* bacterial proteins using STITCH 5.0 revealed a high binding affinity of > 0.7 to DNA and membrane-related proteins. This result unravels the antibacterial properties of *S. crispa* AuNPs, leading to potent bacterial death.

Keywords: gold nanoparticles; *Strobilanthes crispa*; antibacterial activity; *in silico*.

1. Introduction

Nanoscience is a multidisciplinary field concerned with designing and developing functional materials at the molecular level. This applied science focuses on the synthesis, characterization, and application of materials at the nanoscale. Nanoparticles exhibit unique physicochemical properties that can have applications in various fields. Metallic nanoparticles, for example, have attracted much attention due to their excellent properties and wide applications in catalytic, biomedical, optical, and electronic fields [1]. Accordingly, the development of nanoparticle synthesis has received much research attention. Physical and chemical methods are still conventional for preparing metal nanoparticles [2]. However, these

methods have drawbacks such as sophisticated instruments, high economic costs, and hazardous chemical usage that harms the environment and human health. Nanoparticle biosynthesis using plants as a source of green multifunctional chemical agents has been described as an efficient, cost-effective, and environmentally friendly technique to facilitate the synthesis process [3]. Nanomaterials with large surface area and facile functionalization have demonstrated superior physical and chemical properties for catalysis, electronics, and medicine [4]. Recent advances have focused on using metal nanoparticles, including gold and silver, as antibacterial agents against bacterial infections [5, 6]. However, gold nanoparticles (AuNPs) have attracted much interest due to their promising applications in developing novel antibacterial agents [7].

AuNPs are known to be inert non-toxic, and their antibacterial activity does not cause any harmful side effects [8]. This application includes drug delivery, tumor imaging, and even nano-enhancers in diagnostic kits [9]. Usually, the synthesis of AuNPs is carried out by physical and chemical methods [10]. Although there are several chemical synthesis methods for metal nanoparticles, many of the starting materials and precursor chemicals used in these reactions are toxic and hazardous. In addition, most of the physical methods used to produce metal nanoparticles have high energy requirements and require complex instrumentation. Recently, the biogenic method of synthesizing AuNPs using biological resources such as microbes, fungi, and plant extracts has emerged as an alternative to the physical and chemical synthesis routes. This green synthesis method, which uses naturally occurring reducing agents, could be a promising method to replace more complex physiochemical syntheses because green synthesis is free of toxic chemicals and hazardous byproducts and instead uses natural capping agents to stabilize metal nanoparticles [11].

Nowadays, the increasing cases of bacterial infections pose an alarming threat to public health. However, antimicrobial resistance in bacteria continues to increase, making the situation much more challenging due to inadequate antibiotic prescribing and the exchange of resistant genes among different bacterial species [12]. Among the various strategies to overcome antimicrobial resistance is developing new antimicrobial agents. For many years, antibiotics were used primarily to control bacterial infections in the community and hospital settings. However, commercially available antibiotics are not sufficient to destroy mutated bacteria, resulting in antibiotic-resistant bacterial strains. As a result, the antibacterial resistance of pathogenic bacteria has become a significant threat to public health and food safety. A recent report estimated that the number of deaths due to infections caused by antibacterial resistance will increase up to 10 million by 2050, compared to cancer, diabetes, traffic accidents, and other potential diseases [13]. The problem is even more threatening considering the slow development of new antibacterial agents and the limited number of them available compared to the rapid adaptation of pathogens. Nanoparticles are the best candidate for this task due to their large surface area relative to volume and excellent physicochemical properties for catalysis, electronics, and medicine [14].

Therefore, in this study, aqueous extracts of *Strobilanthes crispa* leaves were successfully used to synthesize AuNPs using chloroauric acid as a metal precursor. To date, this is the first study reporting the synthesis of AuNPs from *S. crispa*. *S. crispa*, locally known as pecah kaca or pecah beling, is rich in phytosterols, flavonoids, catechins, alkaloids, caffeine, and tannins [15]. These phytochemicals act as stabilizers or surface capping agents to prevent the aggregation of particles. Moreover, the antibacterial activity of the biosynthesized AuNPs is evaluated using antibacterial assay and STITCH pathway analysis. The combination of *in*

vitro and computational results could further deepen the understanding of the mechanisms of AuNPs towards bacteria.

2. Materials and Methods

2.1. Materials and method.

All laboratory glassware was washed thoroughly with deionized water and dried overnight in an oven. Commercial grade solvents used in the synthesis were dried using appropriate drying agents before the experiment. Milli Q water with a resistivity of more than 18.2 MΩ·cm was used throughout this research. The *S. crispa* leaves were collected in Taman Perling, Johor, Malaysia. Chloroauric acid ($HAuCl_4$) was purchased from Merck. Sodium chloride (NaCl), barium chloride ($BaCl_2$), sulfuric acid (H_2SO_4) were commercially obtained Sigma-Aldrich. Both Nutrient agar (NA) and Mueller Hinton Agar (MHA) powder were obtained from Bacto Difco (BD). All chemicals were used as received without further purification. All samples collected were vacuum dried at room temperature.

2.2. Preparation of leaves extract.

The collected *S. crispa* leaves were washed several times with deionized water to remove any dust or impurities and allowed to dry at room temperature for one week. The dried leaves were then ground into powder using an electrical blender. Then, 2.0 g of leaf powder was added to 100 mL deionized water in a 250 mL beaker, and the mixture was boiled at 100°C for 15 min. The leaves extract solution was then cooled and filtered using a filter paper Whatman® qualitative filter paper (Grade 1). Finally, the *S. crispa* aqueous extract (2% w/v) was kept in a tightly capped reagent glass bottle and stored at 5°C for further use.

2.3. Biosynthesis of gold nanoparticles.

10 mL of 1 mM chloroauric acid, HAuCI4 solution was mixed with 5 mL of *S. crispa* leaves extract (2% w/v) in a glass vial at room temperature. The color of the mixture gradually changed from yellowish to dark brown and finally to reddish-purple within 1 h, indicating the formation of AuNPs [16]. The formation of AuNPs was monitored using UV-Vis spectroscopy for up to 4 hours. The colloidal solution was then centrifuged at 11,000 rpm for 15 min, washed several times using deionized water, and dried in a vacuum desiccator.

2.4. Physicochemical analysis.

The samples were characterized by Ultraviolet-visible (UV-Vis) spectroscopy, Fourier Transform Infrared Spectroscopy (FTIR), X-ray Diffraction (XRD), and High-Resolution Transmission Electron Microscopy (HRTEM). The initial formation of AuNPs by reducing the metal salt solution using the *S. crispa* leaves extract was monitored by using a Shimadzu 2501PC UV-Visible Spectrophotometer operating at a resolution of 1 nm. UV-Vis spectra of the colloidal solution were recorded in a 1 cm path length quartz cuvette in the wavelength range of 200 to 1000 nm. FTIR analysis was carried out to identify the functional groups of the *S. crispa* leaves to powder and the capping agents on the surface of AuNPs. FTIR spectra of synthesized samples were recorded at room temperature on a Perkin-Elmer Spectrum 1600 Fourier Transform-Infrared Spectrometer at a spectral range of 4000-400 cm-1 using potassium bromide (KBr) pressed disk technique. The crystallinity and phase of the biosynthesized

AuNPs were recorded using a Bruker D8 Advance powder diffractometer with Cu-Kα having the wavelength 1.5406 Å operated at 40 kV and 30 mA. The XRD diffraction patterns were recorded in the 2θ range from 10º to 90º. The diffraction patterns were indexed from database files for sample identification and structural confirmation. TEM images were recorded by the HRTEM JEOL JEM-ARM 200F instrument operating at 200 kV. The sample for TEM analysis was prepared by dropping the colloidal AuNPs sample onto a carbon-coated copper grid, vacuum-dried, and loaded into the electron microscopic chamber. The manual analysis to determine the mean diameter was conducted using the Image J software.

2.5. Antibacterial activity of AuNPs.

The antibacterial activity of the biosynthesized AuNPs was assessed against both Gram-positive and Gram-negative bacteria. ATCC cultures of bacteria used were *Staphylococcus aureus* (ATCC 6538) and Gram-negative bacteria *Escherichia coli* (ATCC 11229). For this assay, the disk diffusion technique (DDT) was used to study their antibacterial activity for qualitative and quantitative analyses, respectively. It is an official method developed in 1940 in many clinical microbiology laboratories for routine antimicrobial susceptibility testing [17]. The DDT procedure was performed in triplicates according to the published protocol with some modifications on sample concentration [18]. Firstly, the bacterial was cultured by inoculating colonies of *E. coli* onto nutrient agar plates. This step was carried out in the sterilized biosafety cabinet. Next, the procedure was repeated using *S. aureus*. The plates were incubated for 24 hours and observed their bacterial growth as shown in Figure 1.

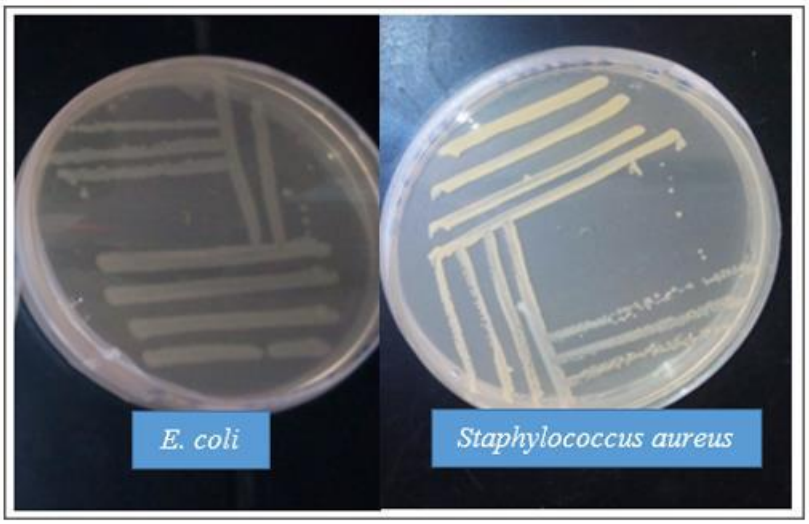

Figure 1. Respective bacterial culture growth with single colonies after 24 hours in an incubator at 37°C.

For the antibacterial test, chloroauric acid (100 µL) with a concentration of 25 mM was used as a positive control for both bacteria. This step is repeated using biosynthesized AuNPs of two concentrations (5 mM and 25 mM). Distilled water and leaves extract was used as a negative control. The bacteria were previously cultured on nutrient agar at 37°C for 24 hours. Next, 3-5 colonies were taken and diluted with sterile 0.9% (w/v) saline solution. The turbidity of a suspension was compared with the turbidity of McFarland standards (1.5 × 108 CFU). An adjustment was made until the turbidity of suspension was equivalent to the McFarland standards. Next, the surface of the Mueller-Hinton Agar (MHA) plate was inoculated with bacterial suspension using a sterile cotton swab by rotating the plate every 60° to confirm homogenous bacteria growth. Next, the previously prepared filter paper disc was placed onto

the bacterial lawn seeded on the surface of the MHA agar, incubating the plate for 24 hours. Finally, the inhibition zone diameter (in cm) was measured to indicate the presence or absence of antibacterial activity.

AuNPs to *E. coli* protein interaction study was done using STITCH 5.0 (Search Tool for Interacting Chemicals). These *in silico* tools were used to understand the possible interaction mechanism. STITCH 5.0 is a continuously expanding pre-computed database resource which offers a protein–chemical interaction network that incorporates many experimental sources, text-mining information, and predictions [19]. There is no information available specifically for *E. coli* ATCC 11229 in the STITCH 5.0 database; hence we used alternative strains *E. coli* ATCC 8739 as protein target. This interaction analysis of AuNPs was set at a high confidence score of 0.7 and above for data filtering and to ensure specificity. This free-resources web interface can be accessed at http://stitch.embl.de.

3. Results and Discussion

3.1. Biosynthesis of AuNPs.

The *S. crispa* aqueous extract's ability to reduce Au(III) to Au(0) was first evaluated. UV-Vis spectroscopy was used to monitor the formation of the resulting AuNPs. This was the preliminary step to investigate whether the biomolecules present in the leaves extract were able and responsible for reducing Au(III) ions to zero-valent AuNPs. The color of the reaction mixture had gradually changed from pale yellow to reddish-purple, as shown in Figure 2. The observed reddish-purple color was attributed to the excitation of surface plasmon resonance which directly indicated the formation of AuNPs and is consistent with previous reports [20, 21].

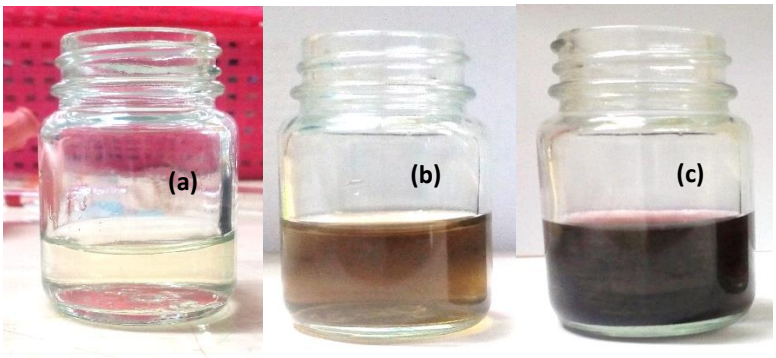

Figure 2. The consecutive color change due to the addition of 5 mL of 2% *S. crispa* aqueous leaves extract to 10 mL of 1 mM Chloroauric Acid, $HAuCl_4$ at the time **(a)** 0 hour, **(b)** 1 hour, **(c)** 2 hours.

Figure 3 shows the UV-Vis spectrum of the colloidal AuNPs solution recorded at different time intervals. The UV-Vis spectrum of the biosynthesized colloidal AuNPs, as seen in Figure 3, clearly shows two absorption peaks. The position of the SPR band could be related to particle size and shape. The appearance of more than a single absorbance in the UV-Vis spectrum could have indicated the presence of anisotropic AuNPs [22]. The stronger and narrower absorption band at a lower wavelength around 530 nm can be assigned to the surface plasmon resonance (SPR) band of spherical and smaller size AuNPs. Previous studies had suggested that the SPR band at 530 nm could be due to AuNPs in spherical morphology [23, 24]. However, the much weaker but broader absorption band centered around 708 nm has been reported to be consistent with the non-spherical shape and larger size of AuNPs [25]. Hence, this result proved the involvement of biomolecules in the *S. crispa* leaves extract, such as

flavonoids and xanthones, in the bioreduction process. Furthermore, these biomolecules also acted as capping agents, leading to anisotropic AuNPs.

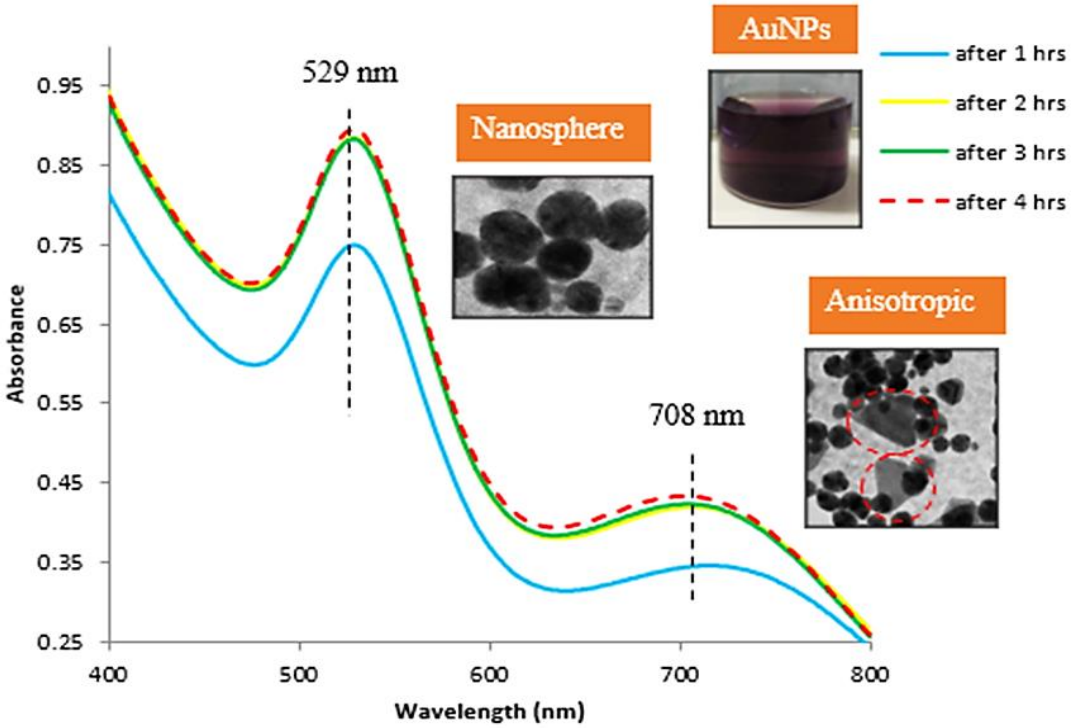

Figure 3. UV-visible spectra of the reaction mixture at different time intervals until saturation.

The plot of absorbance at λmax = 529 nm vs. time (hour) for the AuNPs formation is illustrated in Figure 4 in order to ascertain the time required for the completion of the bioreduction process. As can be seen in Figure 4, the absorbance values gradually increase with time. After 2 hours, it was observed that there was only a small change in the absorbance, suggesting that the bioreduction process had reached completion. This result indicated that the bioreduction of Au (III) to Au (0) using the *S. crispa* leaves extract was completed within 2 hours. Only a few studies had reported the formation of AuNPs in less than 30 minutes [26, 27]. This shows the reaction rate is relatively high and takes several minutes to several hours to complete the reaction was depending on plant type and plant amount.

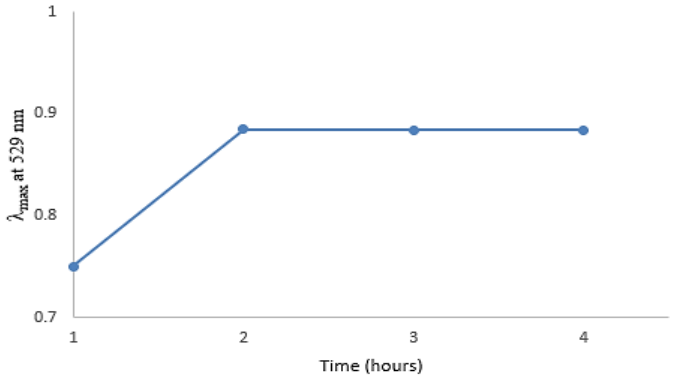

Figure 4. Absorbance against reaction time in the formation of AuNPs.

3.2. Physicochemical analysis.

3.2.1. Fourier Transform Infrared Spectroscopy (FTIR).

FTIR spectroscopy has been used to obtain information on the functional groups of the biomolecules present in the *S. crispa* leaves extract that could reduce the Au^{3+} ions to Au^{0} and

stabilize the AuNPs formed. The FTIR spectra of the *S. crispa* leaf powder and the biosynthesized AuNPs are shown in Figure 5. The FTIR spectrum of *S. crispa* leaf powder showed characteristic bands for O-H stretching vibrations at 3413 cm^{-1}, asymmetric stretching vibrations of C-H at 2923.48 cm^{-1}, stretching vibrations of C=O at 1638 $cm^{-1,}$ and C-O at 1109 cm^{-1} (Table 1). These absorption bands are related to the existence of polyols, carbonyls, and C=C bonds on terpenoids and flavonoids in compounds such as rutin, myricetin, and luteolin identified in *S. crispa* aqueous leaves extract. The broad and strong intensity of the O-H absorption band observed in the FTIR spectrum is due to the abundance of O-H functional groups. The FTIR spectra suggest that the O-H functional group of primary and secondary metabolites mentioned above is most likely responsible for reducing Au^{3+} ions to Au^{0}. Similar findings showed that predominant alkaloids found in *S. crispa* leave extract have acted as weak base sources to provide (OH–), thus reducing colloidal AuNPs. Moreover, saponins and flavonoids were found to stabilize the secondary growth of nanoparticles as a capping agent [28].

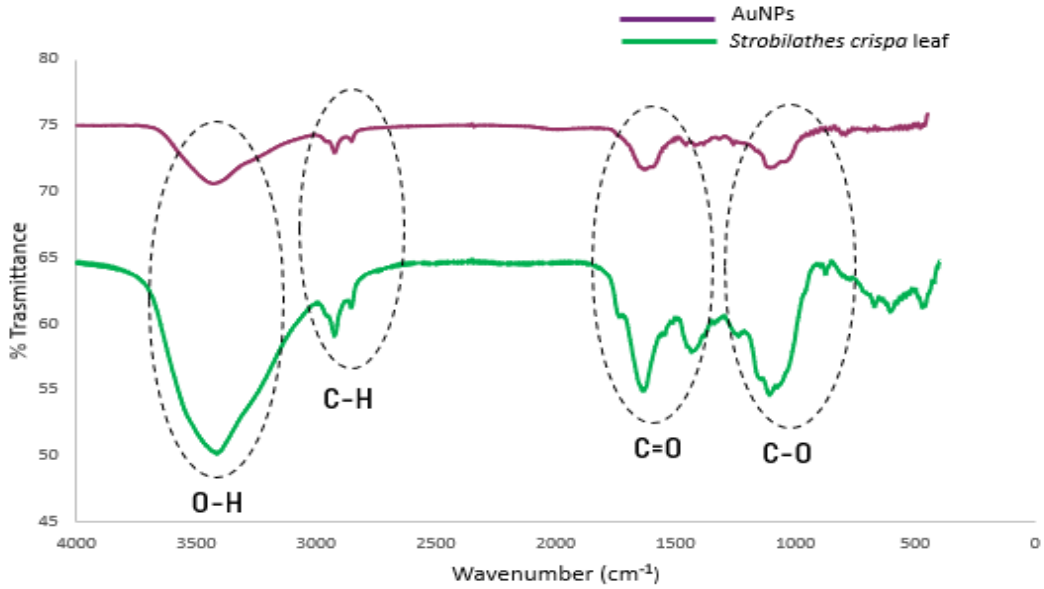

Figure 5. FTIR spectra *Strobilanthes crispa* leaf powder and biosynthesized of AuNPs.

The TIR spectra of the biosynthesized AuNPs and *S. crispa* leaf powder showed similar bands position with different intensities. The FTIR spectrum of the biosynthesized AuNPs showed peaks at 3428 cm^{-1}, 2923 cm^{-1}, 1629 cm^{-1}, and 1106 cm^{-1} demonstrating the presence of O-H, C-H, C=O, and C-O stretching vibrations, respectively (Table 1). This observation suggested the presence of biomolecules capping on the surface of the AuNPs. Hence, these findings proposed that the polyphenols in the leaf extract had acted as a reducing agent and performed the role of surface capping agent to stabilize AuNPs. Furthermore, the much lower absorption intensity of the O-H stretching band in the biosynthesized AuNPs is probably due to the oxidation of catechol moiety of flavonoids such as rutin, myricetin, and luteolin [16].

Table 1. Main IR spectral data of *Strobilanthes crispa* leaf powder and biosynthesized AuNPs.

Type of Bond	**Wavenumber (cm^{-1})**	
	Dried *Strobilanthes crispa* leaf	**AuNPs powder**
O-H	3414	3429
C-H	2923	2925
C=O	1639	1629
C-O	1109	1107

3.2.2. High-Resolution Transmission Electron Microscopy (HRTEM).

HRTEM analysis has been used to identify particle size and morphology of the biosynthesized AuNPs. From the image displayed in Figure 6, it can be observed that the biosynthesized AuNPs mostly exist in spherical morphology. It can be observed that in addition to nanospheres, the biosynthesized AuNPs also exist in other shapes, including nano triangles and nanorods. Anisotropic morphologies of the biosynthesized AuNPs are consistent with the UV-vis spectroscopic analysis. It could explain the presence of two SPR bands in the UV-vis spectrum of the AuNPs. For particle size determination, only the AuNPs with spherical morphology were considered. From 100 particles, the histogram for particle size distribution is plotted as shown in Figure 7(d), and the average particle diameter of AuNPs calculated using image J software is 21.0 nm.

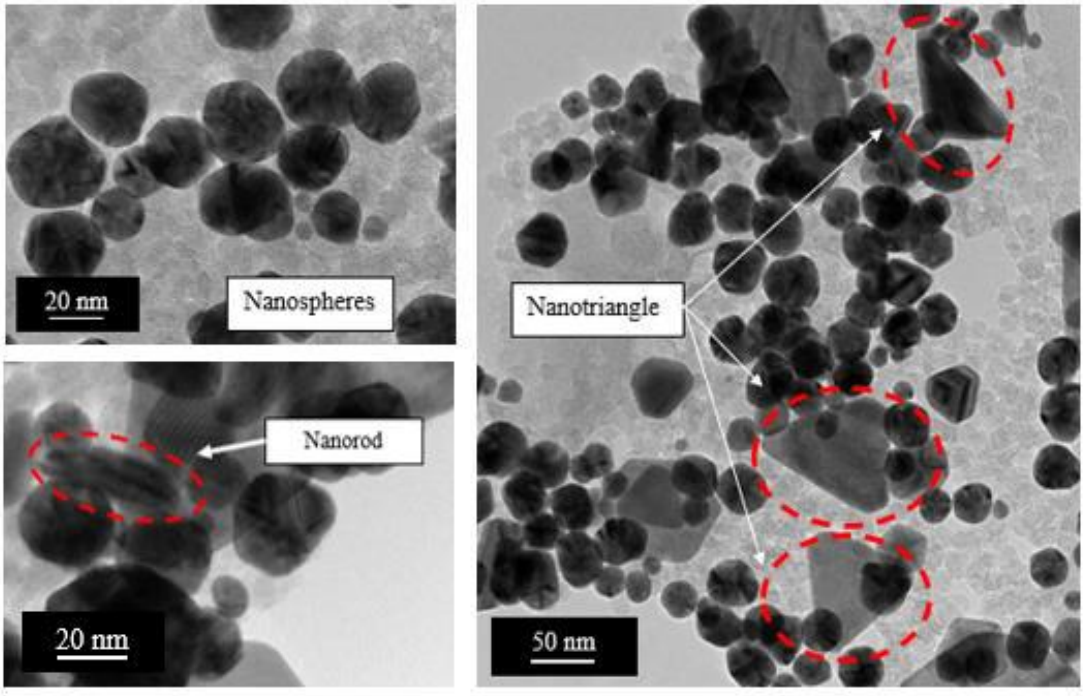

Figure 6. HR-TEM images showing various shapes of AuNPs.

AuNPs of different shapes can be synthesized by anisotropic growth on gold nuclei via a two-step process of seed-mediated growth [29]. In the first step, spherical gold seeds are synthesized with a uniform size. The second step changes the reaction conditions by adding more gold ions, a capping agent, and a reducing agent. The gold seeds prepared in the first step serve as a template on which newly reduced AuNPs are deposited, forming AuNPs of larger size and different shapes. The reducing agent used in the second step is a weak reducing agent, and Au^{3+} can only be converted to Au^{0} in the presence of seeds, which catalyze the reaction. Due to using a weak reducing agent, the second step is a slower process than the first step. The formation of anisotropic AuNPs with different morphologies might be related to the weak reducing agent of *S. crispa* leaves extract.

Several previous studies reported that different morphologies of metallic nanoparticles synthesized with the leaves extract could be formed due to the low nucleation rate, which in turn led to a growth process of the nanoparticles resulting in a much larger particle size when the reducing agent was relatively weak or at low concentration [23]. This result agrees with the study of Ahmad *et al.*, who observed different forms of AuNPs during synthesis using the

extract from the leaves of oil palm *Elaisa guineensis.* He concluded that the predominant contribution of increasing precursor concentration is a factor controlling the initial morphology. Indeed, FTIR analysis revealed that phytochemical compounds such as phenol and carboxyl are important as dual reducing and stabilizing agents in the biosynthesis of AuNPs [30]. Moreover, Ankamwar succeeded in the synthesis of anisotropic AuNPs with multiple twinned pentagonally shaped octahedra and hexagonally shaped icosahedra using the aqueous extract of *Cordia myxa* fruit [31]. Pinto *et al*. also addressed the challenge of controlling the morphology (shapes) and size of biosynthesized AuNPs for large-scale production using green chemistry. He concluded that the extract concentration and pH of the medium play a crucial role in determining the size and morphology of AuNPs when using aqueous *Eucalyptus globulus Labill* bark extract [32].

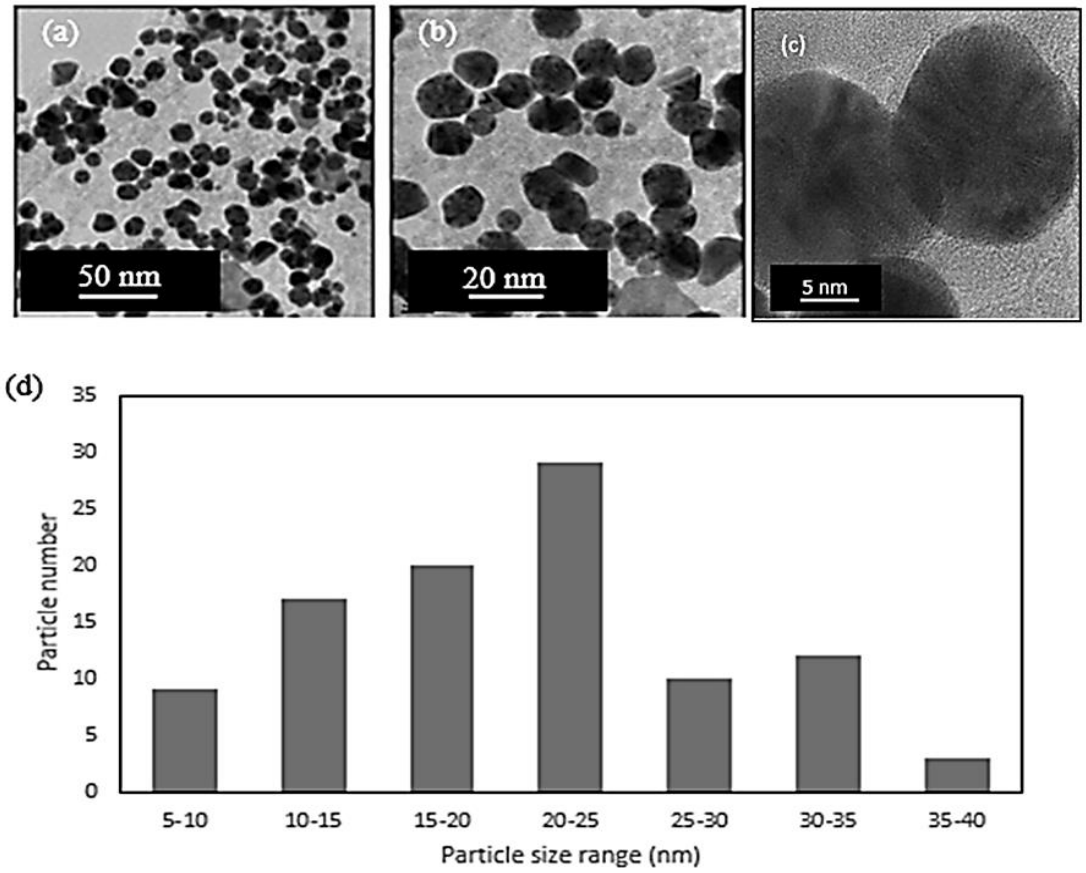

Figure 7. HRTEM images of AuNPs using (**a-c**) different magnifications; (**d**) particle size distribution.

3.2.3. X-ray Diffraction (XRD).

X-ray diffraction analysis of the biosynthesized AuNPs was carried out to examine the crystallinity and phase purity of the biosynthesized sample. As observed in the diffractogram shown in Figure 8, the diffraction peaks appeared at 2θ values of 238.11°, 44.09°, 64.65°, 77.68°, and 81.52°, which correspond to (111), (200), (220), (222) and (311) reflection planes consistent with Au in face-centered cube (fcc) structure (JCPDS database #00-004-0784) and in agreement with literature values [16]. The (111) plane was observed to be more intense than the other planes, suggesting the predominant orientation. The crystallite size of AuNPs was calculated using Debye-Scherer's equation. The most intense peak (111) gives Bragg diffraction angle of 19.053° at wavelength 1.54 Å with full width at half maximum (FWHM) of 0.849. Thus, the crystallite size of AuNPs was calculated at 9.3 nm. The broad hump

observed in the 2θ range of 20 – 30° is due to the amorphous phase depicting the presence of biomolecules from *S. crispa* leaves extracts [33].

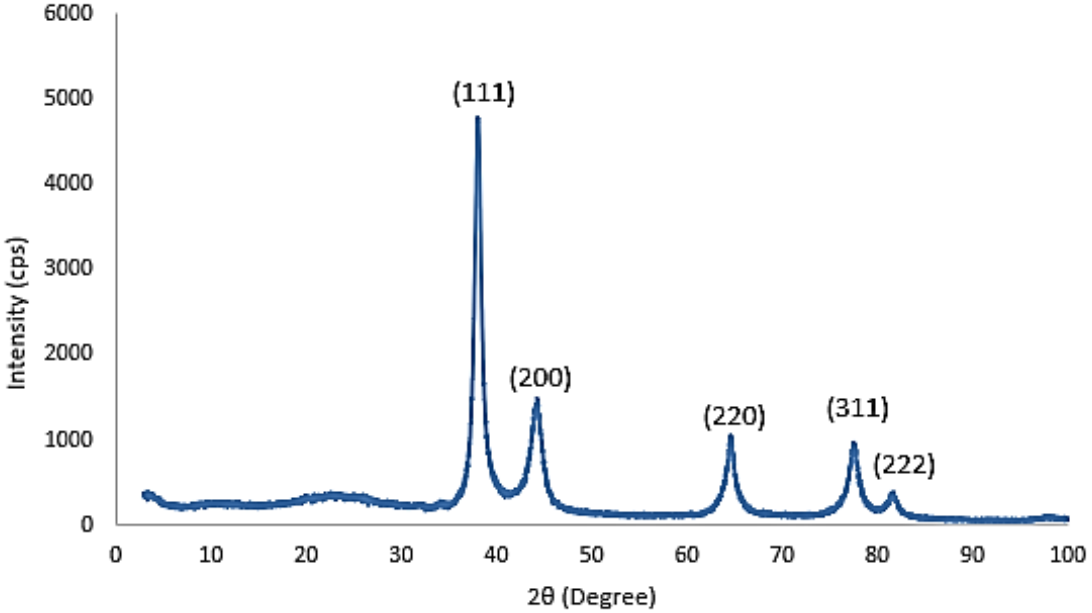

Figure 8. XRD pattern of biosynthesized AuNPs.

3.3. Antibacterial activity evaluation.

3.3.1. Disk-diffusion technique (DDT).

The biosynthesized AuNPs were tested for bacterial activities using the disk diffusion method (DDT). No zone of inhibition was formed in the bacteria treated with *S. crispa* extract as they did not exhibit antibacterial properties, as shown in Figure 9. When the corresponding bacteria were treated with different concentrations of AuNPs, the size of the zone of inhibition also increased, as shown in Figure 10. In this experiment, positive results of the zone of inhibition with AuNPs were shown when tested with *E. coli* with a diameter of 1.8 cm. However, no inhibition zone was observed when tested with *S. aureus*.

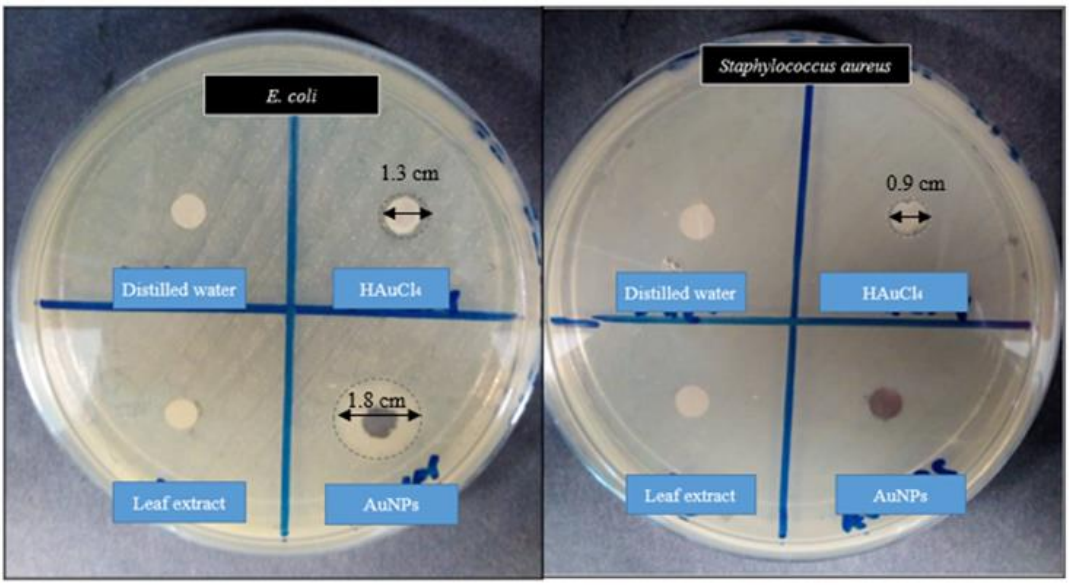

Figure 9. Antibacterial activity for *E. coli* (Gram-negative) and *S. aureus* (Gram-positive).

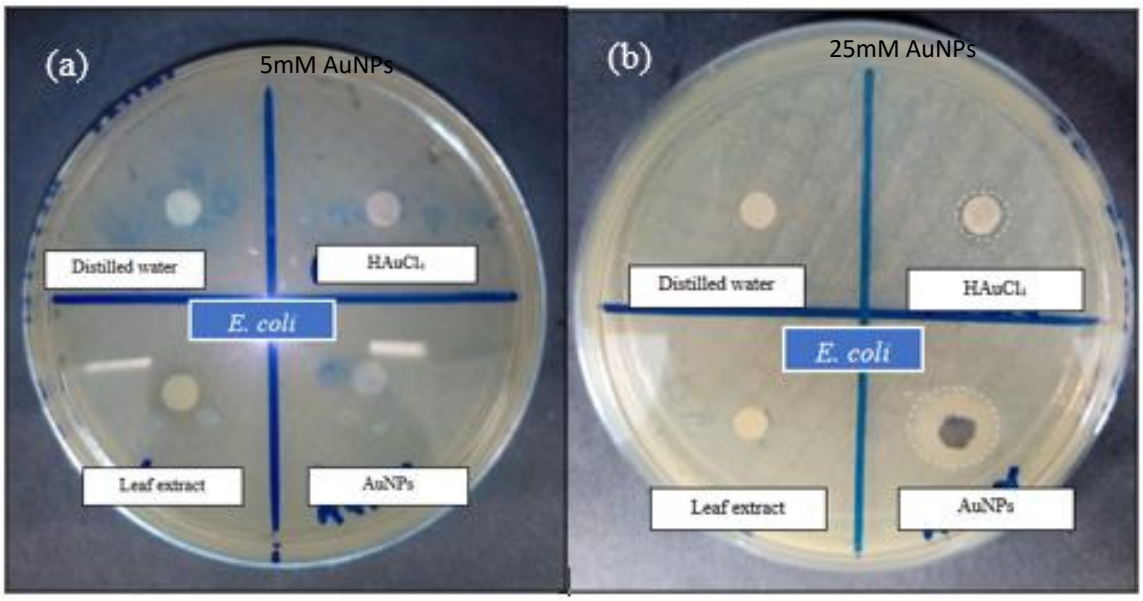

Figure 10. Absent of inhibition zone when using 5 mM AuNPs (b) inhibition zone formed when using 25 mM AuNPs.

There are two main reasons that we can conclude from this observation. The first reason is the difference in cell wall morphology. *E. coli* (Gram-negative) has a thinner cell wall than *S. aureus* (Gram-positive), so AuNPs could easily penetrate the wall of *E. coli* bacteria compared to *S. aureus*. However, AuNPs mainly attack the cell wall or aggregate outside the thick cell wall, so they are unable to destroy Gram-positive bacteria [34] intrinsically. Secondly, the size and concentration of nanoparticles play a major role in killing bacteria [35]. AuNPs have inert properties and thus are known for their biocompatibility, but their cytotoxicity mainly depends on these two factors [36]. The second factor is evident from the antibacterial activity shown in Figure 10: the higher the concentration of AuNPs used, the larger the zone of inhibition. Moreover, this result agrees with that of Katas *et al*. [3], where *S. aureus* requires a high concentration of AuNPs (more than 25 mM) to easily penetrate the cell wall of bacteria due to its thick cell wall. Recent work reported that the antibacterial activity of AuNPs strongly depends on the size, showing the best activity of ultrasmall gold nanoclusters, which can easily penetrate the cell wall pores and massively destroy cell metabolism [37].

Moreover, different forms of AuNPs affect antibacterial activity. After reducing Au (III) with a higher concentration of leaves extract, spherical AuNPs were formed. In contrast, a low extract concentration interacted with Au (III) and produced triangular and other irregular shapes [23]. It has been reported that AuNPs with flower-shaped particles are more effective in killing *S. aureus* than spherical particles due to their protruding ends [3]. Since the spherical shape of the synthesized AuNPs was predominant in this study, the ratio between $HAuCl_4$ and the leaves extract needed to be further modified or optimized to synthesize AuNPs for better antibacterial activity.

3.3.2. *In silico* analysis using STITCH 5.0 (Search Tool for Interacting Chemicals).

To better understand the antibacterial mechanism of AuNPs, it is important to know their binding affinity to bacterial cells using an *in silico* interaction network (STITCH 5.0). Figure 11 shows the comprehensive interaction pathway between AuNPs and bacterial proteins of *E. coli*. The scoring functions between 0.7 and 1.0 are used to evaluate the binding affinities of AuNPs to bacterial proteins. The studies of protein network interactions with *E. coli* revealed

that AuNPs exhibit strong preferential binding to DNA at the cueR and nusA proteins with a confidence value of 0.829 and 0.830, respectively. This halts the transcription process facilitated by cueR and nusA, leading to further defects in protein production in the cell [38].

AuNPs have been shown to disrupt cell membrane permeability by binding to the membrane-associated proteins ybgF (0.818), ykgC (0.811), and aphA (0.800). ybgF, located in the thin periplasmic space of *E. coli* mediates peptidoglycan synthesis and outer membrane formation, whereas ykgC regulates pyridine nucleotide disulfide oxidoreductase, which is an important membrane-bound efflux system in *E. coli* [39].

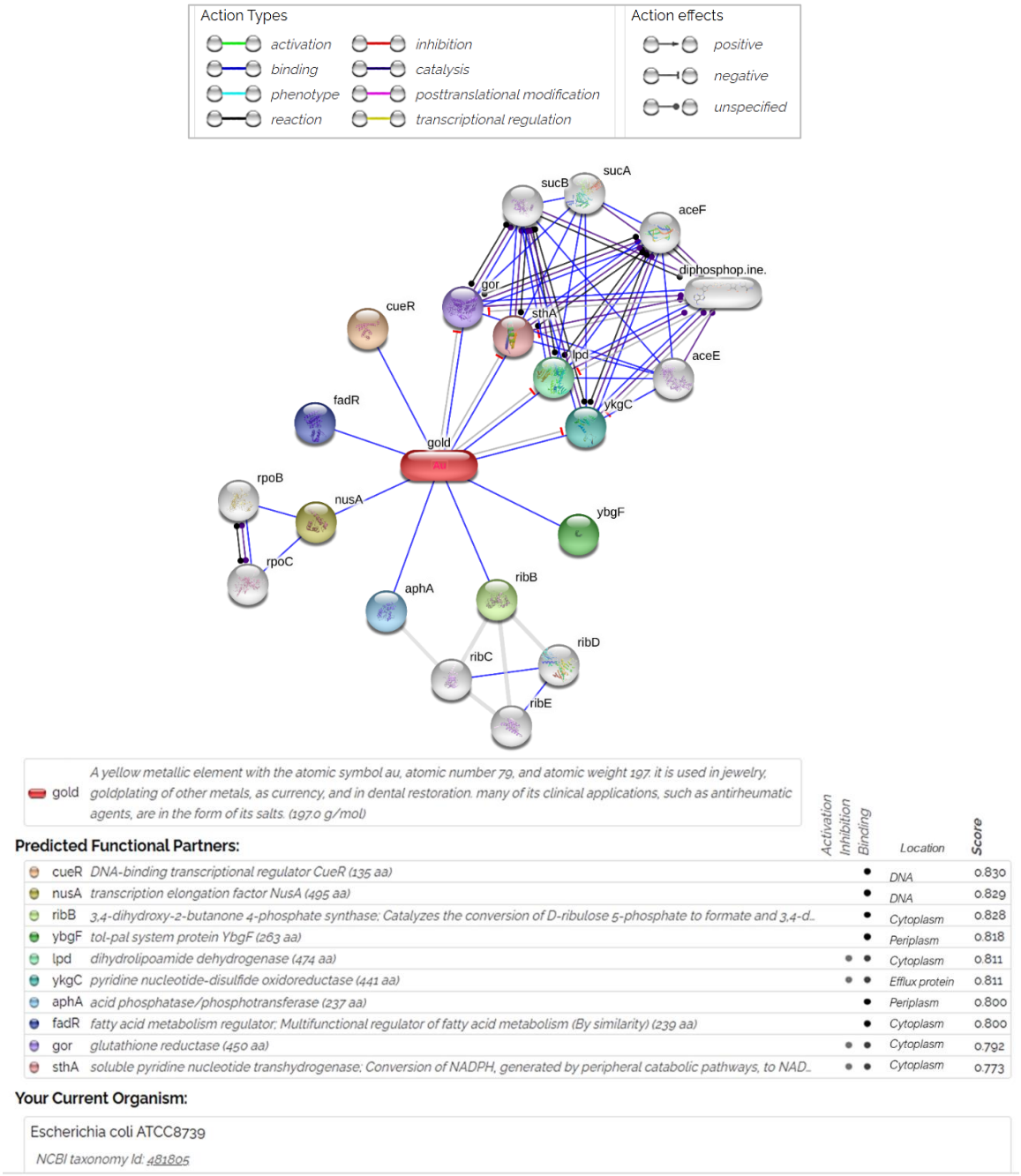

Figure 11. STITCH network mechanism when using input is gold nanoparticle with bacteria *E. coli* ATCC8739.

Due to impaired membrane permeability, rapid uptake of AuNPs into bacterial cells occurs, blocking various metabolic pathways by inactivating proteins such as ribB, lpd, fadR, gor, and sthA. Inactivation of ribB proteins due to increased nanoparticles interferes with

riboflavin biosynthesis and bacterial stress response [40]. AuNPs have also been found to inhibit the gor protein, which maintains cell homeostasis in the cytosol through the presence of reduced glutathione as an intracellular redox buffer. This protein also regulates electrons from NADPH and suppresses oxidative DNA damage [41]. Inhibition of sthA protein can interrupt the conversion of NADPH to NADH for energy production [42].

Interestingly, AuNPs were found to bind and inhibit four major proteins responsible for the cellular response mechanism to oxidative stress (gor, sthA, lpd, and ykgC). Thus, binding to these intrinsic proteins resulted in a significant imbalance due to excessive reactive oxygen species (ROS) production. Finally, oxidative stress is considered an important factor that promotes cell death in response to various signals, thus accelerating the death of bacteria without allowing them to develop resistance [6]. Therefore, *in silico* technique can be used to infer the antibacterial interaction of AuNPs against various bacteria in principle and with high accuracy.

AuNPs have gained popularity due to their antibacterial properties in various applications, including healthcare, cosmetics, and water treatment, which is due to their diverse characteristics and physicochemical properties. Recent studies on the biosynthesis of nanoparticles using *S. crispa* leaves extract, and their applications are listed in Table 2. As summarized in Table 2, there is no report on using this plant from Malaysia to synthesize gold nanoparticles for antibacterial applications. *S. crispa* AuNPs are a promising breakthrough as an antibacterial agent, provided that extensive work is carried out in the future to optimize the biosynthesis process, as the physicochemical properties greatly affect the antibacterial performance of an antibacterial agent.

Table 2. Nanoparticle synthesis using *S. crispa*.

Nanoparticles	Average size	Application	References
AuNPs	25 nm	Antibacterial	This study
AgNPs	Less than 5 µm	*In vitro* antioxidant test	[43]
Chitosan-NPs	132 nm	Antihypercholesterolemia drug	[44]
ZnO-La_2CuO_4	62.1 nm	Photocatalytic degradation of malachite green	[28]
ZnO-La_2O_3	45.59 nm	Photocatalytic degradation of methylene Blue	[45]

4. Conclusions

This study shows that gold nanoparticles could be successfully synthesized from the leaves extract of Strobilanthes *crispa* by a simple, inexpensive, and environmentally friendly approach. Characterization such as UV-Vis, FTIR, HRTEM, and XRD was used to confirm the identity of AuNPs. This biosynthesis took 2 hours and resulted in average particle size of AuNPs of 25 nm. The size of the particles is highly dependent on the amount of leaves extract. HRTEM analysis shows that the AuNPs have a predominantly spherical shape with a 5-40 nm particle size, and the XRD pattern confirms their crystallites. The FTIR spectrum of the leaves extract of *S. crispa*, and the synthesized AuNPs shows the same functional groups. The related bonds refer to the capping biomolecules in the *S. crispa* leaves extract, which plays an important role in the reducing and stabilizing agents. The study of antibacterial activity of AuNPs against human pathogens *E. coli* (Gram-negative) and *Staphylococcus aureus* (Gram-positive) was applied to the biosynthesized AuNPs. From the results, it can be concluded that AuNPs is effective towards *E. coli* with an inhibition zone of 1.8 cm, and the killing mechanism is based on destructive binding to the cell membrane protein, leading to disruption of cell homeostasis and eventual death of bacterial cells, as shown by the analysis of STITCH.

Funding

The authors gratefully acknowledged the financial supports from the Ministry of Higher Education (MOHE) Malaysia and Universiti Teknologi Malaysia (UTM) under the Trans-Disciplinary Research Program UTM-TDR 17.2(T1): Biomediated Shape and Size Control Synthesis of Silver Nanoparticles (AgNPs) using Malaysian Herbal Plant Extract (05G57). AA. Hadi thanked Public Services Department, Malaysia, for a scholarship received through the Excellent Student Program.

Conflicts of Interest

The authors declare no conflict of interest.

Acknowledgments

Declare none.

References

1. Ab Razak, N.H.; Nizam, N.A.; Matmin, J.; Wan Dagang, W.R.Z.; Ahmad Zawawi, N.; Chundawat, T.S. Brief review on bioresources green synthesis of silver nanoparticles. *J. Adv. Res.Mater. Sci.* **2021**, *79*, 1-10.
2. Vijayaraghavan, K.; Ashokkumar, T. Plant-mediated biosynthesis of metallic nanoparticles: A review of literature, factors affecting synthesis, characterization techniques and applications. *J Environ Chem Eng* **2017**, *5*, 4866-4883, https://doi.org/10.1016/j.jece.2017.09.026.
3. Katas, H.; Moden, N.Z.; Lim, C.S.; Celesistinus, T.; Chan, J.Y.; Ganasan, P.; Suleman Ismail Abdalla, S. Biosynthesis and potential applications of silver and gold nanoparticles and their chitosan-based nanocomposites in nanomedicine. *J Nanotechnol* **2018**, *2018*, https://doi.org/10.1155/2018/4290705.
4. Yougbare, S.; Chang, T.-K; Tan, S.-H.; Kuo, J.-C.; Hsu, P.-H.; Su, C.-Y.; Kuo, T.-R.. Antimicrobial gold nanoclusters: recent developments and future perspective. *Int J Mol Sci* **2019**, *20*, 2924, https://doi.org/10.3390/ijms20122924.
5. Sánchez-López, E.; Gomes, D.; Esteruelas, G.; Bonilla, L.; Lopez-Machado, A.L.; Galindo, R.; Cano, A.; Espina, M.; Ettcheto, M.; Camins, A.; Silva, A.M.; Durazzo, A.; Santini, A.; Garcia, M.L.; Souto, E.B. Metal-based nanoparticles as antimicrobial agents: An overview. *Nanomater* **2020**, *10*, 292, https://doi.org/10.3390/nano10020292.
6. Crisan, C.M.; Mocan, T.; Manolea, M.; Lasca, L.I.; Tăbăran, F.A.; Mocan, L. Review on silver nanoparticles as a novel class of antibacterial solutions. *Appl. Sci.* **2021**, *11*, 1120, https://doi.org/10.3390/app11031120.
7. Jha, P.; Saraf, A.; Rath, D.; Sharma, D. Green synthesis and antimicrobial property of gold nanoparticles: A review. *World J Pharm Med Res* **2017**, *3*, 431-435.
8. Piktel, E.; Suprewicz, Ł.; Depciuch, J.; Chmielewska, S.; Skłodowski, K.; Daniluk, T.; Król, G.; Kołat-Brodecka, P.; Bijak, P.; Pajor-Świerzy, A.; Fiedoruk, K.; Parlinska-Wojtan, M.; Bucki, R. Varied-shaped gold nanoparticles with nanogram killing efficiency as potential antimicrobial surface coatings for the medical devices. *Sci rep* **2021**, *11*, 12546, https://doi.org/10.1038/s41598-021-91847-3.
9. Maleki, M.J.; Pourhassan-Moghaddam, M.; Karimi, A.; Akbarzadeh, A.; Zarghami, N.; Mohammadi, S.A. Synthesis, characterisation, and application of chamomile gold nanoparticles in molecular diagnostics: a new component for PCR kits. *Biointerface Res Appl Chem* **2019**, *9*, 4635-4641, http://dx.doi.org/10.33263/BRIAC96.635641.
10. Herizchi, R.; Abasi, E.; Milani, M.; Akbarzadeh, A. Current methods for synthesis of gold nanoparticles. *Artif Cells Nanomed Biotechnol* **2014**, *44*, 596-602, https://doi.org/10.3109/21691401.2014.971807.
11. Lee, S.H.; Jun, B.-H. Silver nanoparticles: Synthesis and application for nanomedicine. *Int J Mol Sci* **2019**, *20*, 865, https://doi.org/10.3390/ijms20040865.
12. Fletcher, S. Understanding the contribution of environmental factors in the spread of antimicrobial resistance. *Environ Health Prev Med* **2015**, *20*, 243-252, https://doi.org/10.1007/s12199-015-0468-0.
13. O'Neill, J. Tackling drug-resistant infections globally: Final report and recommendations. *Government of the United Kingdom* **2016**, https://apo.org.au/node/63983.

14. Wen, A.M.; Steinmetz, N.F. Design of virus-based nanomaterials for medicine, biotechnology, and energy. *Chem Soc Rev* **2016**, *45*, 4074-4126, https://doi.org/10.1039/C5CS00287G.
15. Ng, M.G.; Ng, C.H.; Ng, K.Y., Chye, S.M.; Ling, A.P.K.; Koh, R.Y. Anticancer properties of *Strobilanthes crispus*: A review. *Processes* **2021**, *9*, 1370, https://doi.org/10.3390/pr9081370.
16. Borhamdin, S.; Shamsuddin, M.; Alizadeh, A. Biostabilised icosahedral gold nanoparticles: synthesis, cyclic voltammetric studies and catalytic activity towards 4-nitrophenol reduction. *J Exp Nanosci* **2016**, *11*, 518-530, https://doi.org/10.1080/17458080.2015.1090021.
17. Balouiri, M.; Sadiki, M.; Ibnsouda, S.K. Methods for *in vitro* evaluating antimicrobial activity: A review. *J Pharm Anal* **2016**, *6*, 71-79, https://doi.org/10.1016/j.jpha.2015.11.005.
18. Hadi, A.A.; Ng, J.Y.; Shamsuddin, M.; Matmin, J.; Nik Malek, N.A.N. Green synthesis of silver nanoparticles using *Diplazium esculentum* extract: Catalytic reduction of methylene blue and antibacterial activities. *Chem Pap* **2022**, 76, 65-77, https://doi.org/10.1007/s11696-021-01835-0.
19. Szklarczyk, D.; Santos, A.; von Mering, C.; Jensen, L.J.; Bork, P.; Kuhn, M. STITCH 5: Augmenting protein–chemical interaction networks with tissue and affinity data. *Nucleic Acids Res* **2016**, *44*, D380-D384, https://doi.org/10.1093/nar/gkv1277.
20. Nadaf, N.Y.; Kanase, S.S. Biosynthesis of gold nanoparticles by *Bacillus marisflavi* and its potential in catalytic dye degradation. *Arab J Chem* **2019**, *12*, 4806-4814, https://doi.org/10.1016/j.arabjc.2016.09.020.
21. Oueslati, M.H.; Tahar, L.B.; Harrath, A.H. Catalytic, antioxidant and anticancer activities of gold nanoparticles synthesized by kaempferol glucoside from *Lotus leguminosae*. *Arab J Chem* **2020**, *13*, 3112-3122, https://doi.org/10.1016/j.arabjc.2018.09.003.
22. Wong, S.T.; Shamsuddin, M.; Alizadeh, A.; Yun, Y.S. In-situ generated palladium seeds lead to single-step bioinspired growth of Au-Pd bimetallic nanoparticles with catalytic performance. *Mater Chem Phys* **2016**, *183*, 356-365, https://doi.org/10.1016/j.matchemphys.2016.08.039.
23. Aldewachi, H.; Chalati, T.; Woodroofe, M.N.; Bricklebank, N.; Sharrack, B.; Gardiner, P. Gold nanoparticle-based colorimetric biosensors. *Nanoscale* **2018**, *10*, 18-33, https://doi.org/10.1039/C7NR06367A.
24. Srinath, B.S.; Ravishankar Rai, V. Biosynthesis of highly monodispersed, spherical gold nanoparticles of size 4-10 nm from spent cultures of *Klebsiella pneumoniae*. *3 Biotech* **2015**, *5*, 671-676, https://doi.org/10.1007/s13205-014-0265-2.
25. Hong, Y.; Jing, X.; Huang, J.; Sun, D.; Odoom-Wubah, T.; Yang, F.; Du, M.; Li, Q. Biosynthesized bimetallic Au–Pd nanoparticles supported on TiO_2 for solvent-free oxidation of benzyl alcohol. *ACS Sustain Chem Eng* **2014**, *2*, 1752-1759, https://doi.org/10.1021/sc500181z.
26. Chahardoli, A.; Karimi, N.; Sadeghi, F.; Fattahi, A. Green approach for synthesis of gold nanoparticles from *Nigella arvensis* leaf extract and evaluation of their antibacterial, antioxidant, cytotoxicity and catalytic activities. *Artif Cells Nanomed Biotechnol* **2018**, *46*, 579-588, https://doi.org/10.1080/21691401.2017.1332634.
27. Noruzi, M. Biosynthesis of gold nanoparticles using plant extracts. *Bioprocess Biosyst Eng* **2015**, *38*, 1-14, https://doi.org/10.1007/s00449-014-1251-0.
28. Yulizar, Y.; Apriandanu, D.O.B.; Ashna, R.I. La_2CuO_4-decorated ZnO nanoparticles with improved photocatalytic activity for malachite green degradation. *Chem Phys Lett* **2020**, *755*, 137749, https://doi.org/10.1016/j.cplett.2020.137749.
29. Bandyopadhyay, S.; McDonagh, B.H.; Singh, G.; Raghunathan, K.; Sandvig, A.; Sandvig, I.; Andreassen, J-P.; Glomm, W.R. Growing gold nanostructures for shape-selective cellular uptake. *Nanoscale Res Lett* **2018**, *13*, 254, https://doi.org/10.1186/s11671-018-2662-7.
30. Ahmad, T.; Irfan, M.; Bhattacharjee, S. Parametric study on gold nanoparticle synthesis using aqueous *Elaise guineensis* (oil palm) leaf extract: Effect of precursor concentration. *Procedia Eng* **2016**, *148*, 1396-1401, https://doi.org/10.1016/j.proeng.2016.06.558.
31. Ankamwar, B.; Salgaonkar, M.; Sur, U.K. Room temperature green synthesis of anisotropic gold nanoparticles using novel biological fruit extract. *Inorg Nano-Metal Chem* **2017**, *47*, 1359-1363, https://doi.org/10.1080/24701556.2017.1284121.
32. Pinto, R.J.B.; Lucas, J.M.F.; Morais, M.P.; Santos, S.A.O.; Silvestre, A.J.D.; Marques, P.A.A.P.; Freire, C.S.R. Demystifying the morphology and size control on the biosynthesis of gold nanoparticles using *Eucalyptus globulus* bark extract. *Ind Crops Prod* **2017**, *105*, 83-92, https://doi.org/10.1016/j.indcrop.2017.05.003.
33. Fernandes, M.C.; Sellappan, K. Elemental composition and x-ray diffraction studies of *Strobilanthes* species. *Indian J Biochem Biophys* **2019**, *56*, 144-149, http://nopr.niscair.res.in/handle/123456789/46915.

34. Xu, Y.; Wang, H.; Zhang, M.; Zhang, J.; Yan, W. Plasmon-enhanced antibacterial activity of chiral gold nanoparticles and *in vivo* therapeutic effect. *Nanomater* **2021**, *11*, 1621, https://doi.org/10.3390/nano11061621.
35. Abdelsattar, A.S.; Dawoud, A.; Helal, M.A. Interaction of nanoparticles with biological macromolecules: A review of molecular docking studies. *Nanotoxicol* **2021**, *15*, 66-95, https://doi.org/10.1080/17435390.2020.1842537.
36. Coradeghini, R.; Gioria, S.; García, C.P.; Nativo, P.; Franchini, F.; Gilliland, D.; Ponti, J.; Rossi, F. Size-dependent toxicity and cell interaction mechanisms of gold nanoparticles on mouse fibroblasts. *Toxicol Lett* **2013**, *217*, 205-216, https://doi.org/10.1016/j.toxlet.2012.11.022.
37. Zheng, K.; Setyawati, M.I.; Leong, D.T.; Xie, J. Overcoming bacterial physical defenses with molecule-like ultrasmall antimicrobial gold nanoclusters. *Bioactive materials* **2020**, *6*, 941-950, https://doi.org/10.1016/j.bioactmat.2020.09.026.
38. Kisiela, D.I.; Radey, M.; Paul, S.; Porter, S.; Polukhina, K.; Tchesnokova, V.; Shevchenko, S.; Chan, D.; Aziz, M.; Johnson, T.J.; Price, L.B.; Johnson, J.R.; Sokurenko, E.V. Inactivation of transcriptional regulators during within-household evolution of *Escherichia coli*. *J Bacteriol* **2017**, *199*, e00036-17, https://doi.org/10.1128/JB.00036-17.
39. Anuj, S.A.; Gajera, H.P.; Hirpara, D.G.; Golakiya, B.A. Bacterial membrane destabilization with cationic particles of nano-silver to combat efflux-mediated antibiotic resistance in Gram-negative bacteria. *Life Sci* **2019**, *230*, 178-187, https://doi.org/10.1016/j.lfs.2019.05.072.
40. Pedrolli, D.; Langer, S.; Hobl, B.; Schwarz, J.; Hashimoto, M.; Mack, M. The ribB FMN riboswitch from *Escherichia coli* operates at the transcriptional and translational level and regulates riboflavin biosynthesis. *FEBS J* **2015**, *282*, 3230-3242, https://doi.org/10.1111/febs.13226.
41. Smirnova, G.; Muzyka, N.; Lepekhina, E.; Oktyabrsky, O. Roles of the glutathione- and thioredoxin-dependent systems in the *Escherichia coli* responses to ciprofloxacin and ampicillin. *Arch Microbiol* **2016**, *198*, 913-921, https://doi.org/10.1007/s00203-016-1247-z.
42. Dziva, F.; Hauser, H.; Connor, T.R.; van Diemen, P.M.; Prescott, G.; Langridge, G.C.; Eckert, S.; Chaudhuri, R.R.; Ewers, C.; Mellata, M.; Mukhopadhyay, S. *et al.* Sequencing and functional annotation of avian pathogenic *Escherichia coli* serogroup O78 strains reveal the evolution of *E. coli* lineages pathogenic for poultry via distinct mechanisms. *Infect Immun* **2013**, *81*, 838-849, https://doi.org/10.1128/iai.00585-12.
43. Hong, C.C. Biogenic synthesis and characterization of silver nanoparticles using *Strobilanthes crispus* and in-vitro determination of antioxidant activity. Undergraduate Final Year Project Report **2018**, Universiti Malaysia Kelantan, Malaysia, http://umkeprints.umk.edu.my/id/eprint/11210.
44. Aini, D. Q., Arbianti, R., Utami, T.S. Inhibition and released profile assay of nasty shard nanoparticle leaves extract *Strobilanthes crispus* as drug dosage formulation of antihypercholesterolemia. Degree Dissertation **2015**, Universitas Indonesia, http://www.lontar.ui.ac.id/detail?id=20411516&lokasi=lokal.
45. Ashna, R.I.; Yulizar, Y.; Apriandanu, D.O.B. *Strobilanthes crispus* (B.) leaf extract-assisted green synthesis of ZnO-La_2O_3 composite and preliminary study of its photocatalytic activity. *In IOP Conference Series: Materials Science and* Engineering, 3rd International Symposium on Current Progress in Functional Materials, Depok, Indonesia, 8-9 August 2018, IOP Publishing Ltd. **2020**; *763*, 012004, https://doi.org/10.1088/1757-899X/763/1/012004.